Inorganic Chemistry

ARTICLE

pubs.acs.org/IC

Effective Octadecylamine System for Nanocrystal Synthesis

Dingsheng Wang and Yadong Li*

Department of Chemistry, Tsinghua University, Beijing 100084, P. R. China

Supporting Information

ABSTRACT: New chemical reactions and synthetic systems are of key importance for materials fabrication. In this work, we reported a facile and effective octadecylamine (ODA) synthetic system for various nanocrystals including metals, mixed metal oxides, metal/metal oxide heterostructured nanocrystals, intermetallics, and alloys. We found that the products were mainly determined by metal ions used in our synthetic system: noble metal ions led to the formation of metals; two kinds of non-noble metal ions led to the formation of mixed metal oxides; silver ions and non-noble metal ions led to the formation of metal/metal oxide heterostructured nanocrystals; non-noble metal ions and noble metal (excluding Ag) ions led to the formation of intermetallics and alloys. The difference was attributed to different ability to attract electrons from ODA solvent among these metal ions. This effective system provides a general strategy for various nanocrystals which would find potential applications in many significant fields.

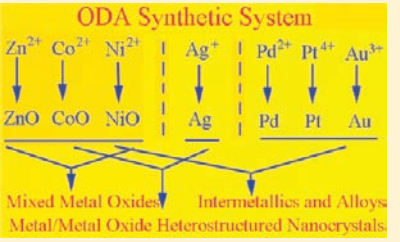

INTRODUCTION

As we know, at the nanoscale, materials exhibit very interesting size- and shape-dependent optical, electrical, magnetic, and chemical properties that differ drastically from the bulky ones.[1−5] Therefore, synthesis of nanomaterials has been among the key research topics in the field of nanoscience and nanotechnology over the past decades.[6−15] Up to now, worldwide scientists in nanorelated fields have achieved successful synthesis of nearly all kinds of nanomaterials with controllable composition, structure, size, and morphology.[16−29] However, given the demand in future industrial applications of nanomaterials, much effort is still required in the exploration of new synthetic process for large-scale synthesis of nanocrystals in a facile, efficient, and economical way.

In 1993, high-quality cadmium chalcogenide semiconductor quantum dots were successfully synthesized by Murray, Norris, and Bawendi for the first time.[30] The method involved the injection of a "cold" solution of precursor molecules (organometallic $CdMe_2$ and TOPSe) into a hot coordinating alkyl solvent (TOPO). This hot-injection method represented a clear break with previous wet-synthetic methods, which opened the door to wide preparation of high-quality monodisperse nanocrystals. In the following years, many research groups proposed numerous adaptations to this synthesis route.[31−38] Monodisperse metal, semiconductor, and metal oxide nanocrystals were synthesized using various organometallic precursors (metal acetylacetonates, metal cupferronates, metal alkoxides, metal carbonyls, etc.) and mixed organic solvents (TOPO, HPA, oleic acid, oleylamine, hexadecanediol, dodecanethiol, etc.) in an inert atmosphere. However, complex operation, high cost, and low production limited the industrial applications of nanocrystals.

Recently, we developed an improved hot-injection method for the preparation of monodisperse Ag nanoparticles and transition metal oxide nanocrystals.[39] In our synthesis, inorganic salts (metal nitrates) were used as precursors and ODA was adopted as single solvent functioning simultaneously as surfactant and reducing agent. The reaction was performed in air and finished within a few minutes. Now, the question is why different metal ions lead to the formation of different kinds of products in ODA solvent. According to the investigation results of Alivisatos' group,[40] ODA can offer electrons at an elevated temperature (eq 1). So, the ODA solvent has some reducing power at high temperature, and the ability to attract electrons of metal ions determines the products. As we know, the order of the ability to attract electrons of metal ions is $Zn^{2+} < Co^{2+} < Ni^{2+} < Ag^{+} < Pd^{2+} < Pt^{4+} < Au^{3+}$.[41] Since Ni^{2+} cannot attract electrons from ODA and thus NiO is the product, it is easy to understand that all metal ions whose abilities to attract electrons are weaker than that of Ni^{2+} cannot be reduced and corresponding metal oxides are the products. Since Ag^{+} can attract electrons from ODA and is reduced to Ag, we can deduce that all metal ions whose abilities to attract electrons are stronger than that of Ag^{+} can be reduced to metals (eq 2). Furthermore, various nanomaterials can be synthesized when two kinds of inorganic salts are used as reactants together in this electron-rich system. If we introduce two kinds of non-noble metal inorganic salts into this system, mixed metal oxide nanocrystals (Ni−Co−O, Zn−Co−O, Cu−Mn−O, etc.) will be obtained (eq 3), if we introduce $AgNO_3$ and non-noble metal inorganic salts into this system, metal/metal oxide heterostructured nanocrystals (Ag−CoO, Ag−NiO, Ag−Fe_2O_3, etc.) will be obtained (eq 4), and if we introduce noble metal (excluding Ag) inorganic salts and non-noble metal inorganic salts into this system, intermetallic and alloyed

Received: March 9, 2011
Published: May 11, 2011

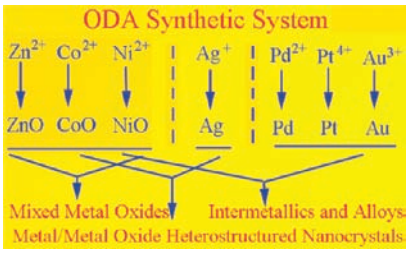

Figure 1. Synthesis of various nanocrystals in ODA solvent.

nanocrystals ($CdPt_3$, $ZnPt_3$, $CoPd_2$, CoRh, CuRh, NiRu, etc.) will be obtained (eq 5). All the results are summarized in Figure 1.

$$RNH_2 \xrightarrow{\Delta} RNH_2^+ + e^- \quad (1)$$

$$M^{x+} \xrightarrow{ODA} M\ (M = Ag, Au, Pd, Pt, Ir, Rh, Ru, etc.) \quad (2)$$

$$M^{x+} + N^{y+} \xrightarrow{ODA} M - N - O\ (M, N = Mn, Fe, Co, Ni, Cu, Zn, etc.) \quad (3)$$

$$M^{x+} + N^{y+} \xrightarrow{ODA} M - NO\ (M = Ag;\ N = Mn, Fe, Co, Ni, Cu, Zn, etc.) \quad (4)$$

$$M^{x+} + N^{y+} \xrightarrow{ODA} MN\ (M = Au, Pd, Pt, Ir, Rh, Ru, etc.;\ N = Mn, Fe, Co, Ni, Cu, Zn, etc.) \quad (5)$$

EXPERIMENTAL SECTION

Synthesis of Noble Metal Nanocrystals. All the reagents used in this work, including various kinds of metal inorganic salts, ODA, ethanol, and cyclohexane, were of analytical grade from the Beijing Chemical Factory, China.

In a typical synthesis of Au nanocrystals, 10 mL of ODA was added into a 50 mL beaker in air. The resulting solution was heated up to 160 °C, and then 0.05 g of $HAuCl_4$ was added. The mixture was magnetically stirred for 10 min. After reaction, particles were collected at the bottom of the beaker. The collected products were washed several times with ethanol and then dispersed in nonpolar solvent such as cyclohexane.

Synthesis of Mixed Metal Oxide Nanocrystals. In a typical synthesis of Ni−Co−O nanocrystals, 10 mL of ODA was added into a 50 mL beaker in air. The resulting solution was heated up to 200 °C, and then 1 mmol of $Ni(NO_3)_2$ and 1 mmol of $Co(NO_3)_2$ were added. The mixture was magnetically stirred for 10 min. After reaction, products were collected at the bottom of the beaker.

Synthesis of Metal/Metal Oxide Heterostructured Nanocrystals. In a typical synthesis of Ag/CoO nanocrystals, 10 mL of ODA was added into a 50 mL beaker in air. The resulting solution was heated up to 200 °C, and then 1 mmol of $AgNO_3$ and 1 mmol of $Co(NO_3)_2$ were added. The mixture was magnetically stirred for 10 min. After reaction, products were collected at the bottom of the beaker.

Synthesis of Intermetallic and Alloyed Nanocrystals. In a typical synthesis of $CoPd_2$ nanocrystals, 10 mL of ODA was added into a 50 mL beaker in air. The resulting solution was heated up to 160 °C. Then, 0.2 mmol of $PdCl_2$ and 0.1 mmol of $Co(NO_3)_2$ were added. After the reactants were dissolved, the system was heated up to 280 °C. The mixture was magnetically stirred for 10 min at this temperature. After reaction, products were collected at the bottom of the beaker.

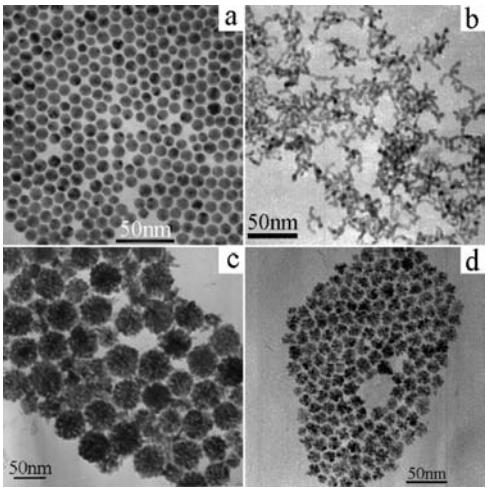

Figure 2. TEM images of (a) Au, (b) Pd, (c) Pt, and (d) Ir nanocrystals.

Characterization of Products. Powder X-ray diffraction (XRD) patterns of all the products obtained in this work were recorded with a Bruker D8-advance X-ray powder diffractometer with monochromatized Cu Kα radiation (λ = 1.5406 Å). The size and morphology of all the products synthesized in this work were determined by using Hitachi model H-800 transmission electron microscope (TEM), JSM-6301F scanning electron microscope (SEM), and JEOL-2010F high-resolution transmission electron microscope (HRTEM). The specimen was prepared as follows: a small amount of product was dispersed in cyclohexane, and then one drop of the resulting suspension was transferred onto a standard holey carbon-covered copper microgrid and dried at room temperature in air.

RESULTS AND DISCUSSION

Noble Metal Nanocrystals. We employ synthesis of Au nanoparticles as an example to introduce the preparation of noble metal nanocrystals in ODA system (eq 2). In our synthesis, $HAuCl_4$ was dissolved in a warm solvent of ODA. After 10 min of magnetic stirring, nearly monodisperse Au nanoparticles could be obtained. Figure S1 (Supporting Information) shows the XRD pattern of as-synthesized Au nanocrystals. The peaks at 38.2°, 44.4°, 64.6°, and 77.6° 2θ correspond to the (111), (200), (220), and (311) reflections of Au, respectively (JCPDS 65-2870). Slight peak broadening of the XRD peaks was primarily due to the small particle size. TEM image of the products is depicted in Figure 2a. We can see that as-obtained Au nanoparticles have an average diameter of 10 nm. The synthetic process for other noble metal nanocrystals was similar to that for Au nanoparticles. Figure 2b shows the TEM image of as-synthesized Pd nanocrystals which display worm-like morphology with an average diameter of 5 nm and a length of 20−50 nm. Pt nanocrystals obtained in the ODA system show spherical morphology (Figure 2c). These Pt spheres have an average size of 50 nm and consist of smaller particles. Figure 2d shows the TEM image of as-synthesized Ir nanoflowers with an average size of 20 nm. Ru and Rh nanocrystals could also be prepared in this synthetic system when $RuCl_3$ and $RhCl_3$ were used as the reactants, respectively.

We note that the order of the ability to attract electrons of metal ions is $Pd^{2+} < Pt^{4+} < Au^{3+}$, indicating that Au^{3+} has a greater tendency to attract electrons from ODA solvent than Pd^{2+}

dx.doi.org/10.1021/ic200485v |Inorg. Chem. 2011, 50, 5196–5202

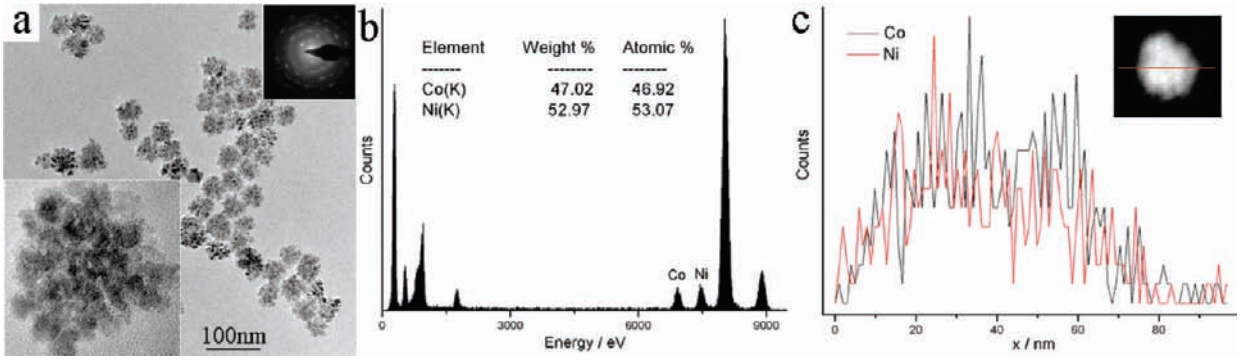

Figure 3. (a) TEM image and (b) EDS spectrum of Ni−Co−O nanocrystals. (c) The line elemental EDS data across one single sphere.

and Pt^{4+}. So, under the same condition, Au^{3+} should be more easily reduced than Pd^{2+} and Pt^{4+}, which has been confirmed by the preceding experimental results. In the ODA system, Au nanocrystals can be obtained at temperature as low as 160 °C, while the reaction temperatures for Pd and Pt are 220 and 200 °C, respectively.

Mixed Metal Oxide Nanocrystals. When two kinds of non-noble metal inorganic salts were used as the reactants simultaneously, mixed metal oxide nanocrystals could be prepared in the ODA system (eq 3). For example, after 1:1 molar ratio of $Ni(NO_3)_2$ and $Co(NO_3)_2$ were dissolved in a warm solvent of ODA, 10 min of magnetic stirring at 200 °C led to the formation of Ni−Co−O nanocrystals. The typical TEM image of Ni−Co−O nanocrystals is depicted in Figure 3a. We can see that nearly monodisperse Ni−Co−O spheres with an average diameter of 50 nm could be obtained via this facile strategy. From the HRTEM image of a single sphere (Figure 3a, inset), it is obvious that these spheres are composed of smaller nanoparticles. The SAED pattern (Figure 3a, inset) also confirms that the sphere is polycrystalline. An EDS experiment was performed on an as-synthesized sample. From the spectrum shown in Figure 3b, we can see that Ni and Co peaks can be observed together, and the composition confirmed by EDS is nearly $Ni_{0.53}Co_{0.47}O$. The line elemental EDS data (Figure 3c) across one single sphere show a rather homogeneous distribution of both Ni and Co in each sphere.

Since both Ni^{2+} and Co^{2+} cannot be reduced by ODA solvent, it is easy to understand the formation of mixed metal oxides when Ni and Co salts react in the ODA system. Similarly, we can also synthesize other mixed metal oxide nanocrystals. Figure S2 (Supporting Information) shows the TEM images of as-obtained Zn−Co−O, Cu−Co−O, Cu−Mn−O, and Ni−Mn−O nanocrystals. Additionally, we can even synthesize trimetallic mixed oxide nanocrystals (e.g., $Co_xNi_yMn_zO$) by using three kinds of transition metal inorganic salts as precursors. These mixed metal oxide nanocrystals are believed to be applicable in Li ion battery as electrode materials or in catalysis as the supports.

Metal/Metal Oxide Nanocrystals. If $AgNO_3$ and non-noble metal inorganic salts (e.g., $Co(NO_3)_2$, $Ni(NO_3)_2$, $Fe(NO_3)_3$, etc.) were used as the reactants together, we could synthesize metal/metal oxide heterostructured nanocrystals (Ag−CoO, Ag−NiO, Ag−Fe_2O_3, etc.) in the ODA system (eq 4). Here, we take Ag−CoO as an example to describe the results. The XRD pattern in Figure S3 (Supporting Information) shows the resulting products composed of Ag and CoO mixture. From the EDS spectrum shown in Figure 4b, we can see that only Ag, Co, and O peaks are observed together with the Cu peak which was

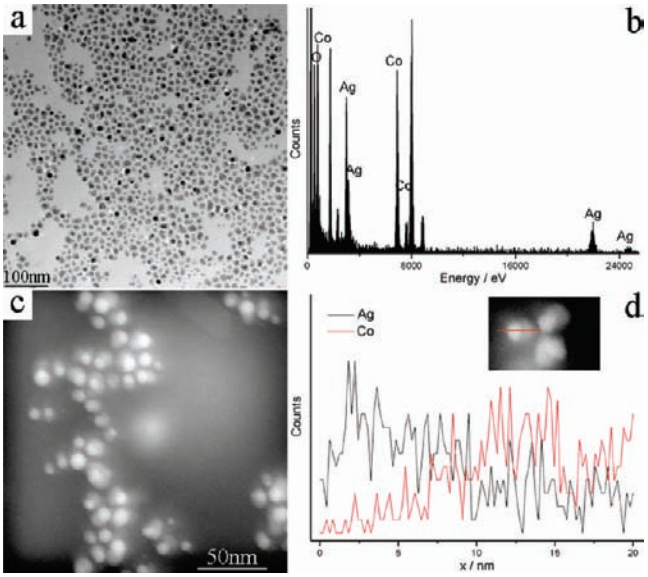

Figure 4. (a) TEM image, (b) EDS spectrum, and (c) HAADF-STEM image of Ag/CoO nanocrystals. (d) The line elemental EDS data across one single particle.

generated by the copper grid, further confirming the composition of as-obtained samples. TEM image (Figure 4a) and high-angle annular dark-field scanning transmission electron microscopy (HAADF-STEM) image (Figure 4c) display Ag/CoO nanocrystals showing spindlelike morphology. The line elemental EDS data (Figure 4d) across a single particle further confirm that the tip is Ag and the tail is CoO.

As we know, noble metal supported catalysts are the most important catalysts in industrial applications. The traditional preparation method for noble metal supported catalysts usually contains two steps. The first step is to synthesize noble metal nanoparticles and metal oxide nanocrystals (used as the supports), respectively. The next step is to load noble metal nanoparticles onto the supports. Synthesis of metal/metal oxide nanocrystals in the ODA system provides a one-step method for preparation of noble metal supported catalysts which will find applications in catalysis.

Intermetallic and Alloyed Nanocrystals. Because Ag^+ can be reduced while non-noble metal ions cannot be reduced by ODA solvent, it is also easy to understand the formation of Ag/metal oxide nanocrystals when Ag^+ and non-noble metal ions

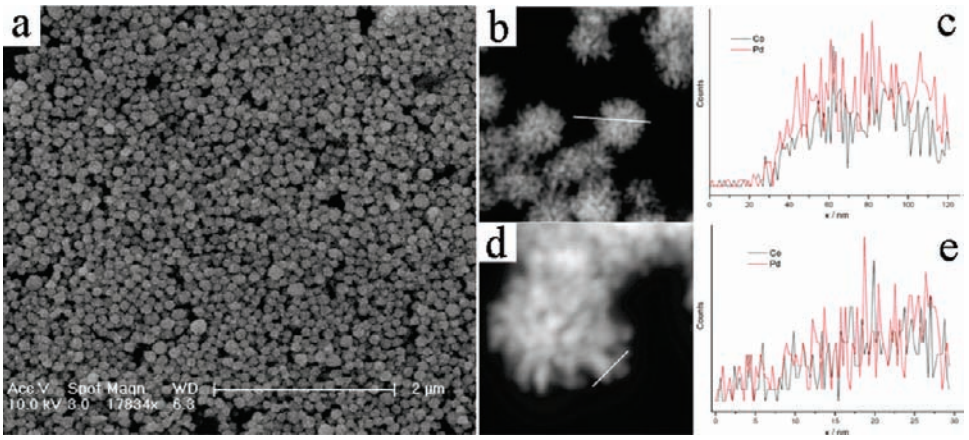

Figure 5. (a) SEM image of $CoPd_2$ nanocrystals; (b and d) HAADF-STEM images of $CoPd_2$ nanocrystals. (c) The elemental profiles for Co and Pd obtained by recording EDS signal intensities along the line shown in part b; (e) the elemental profiles for Co and Pd obtained by recording EDS signal intensities along the line shown in part d.

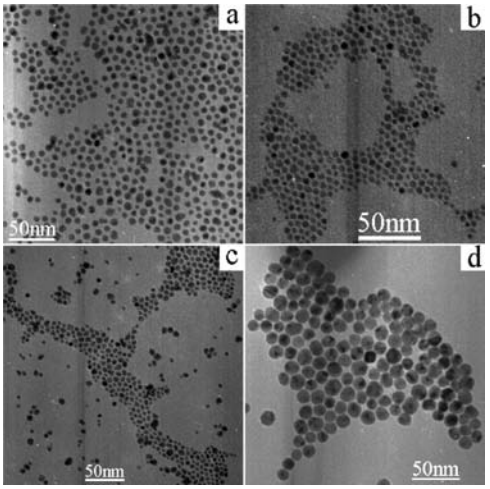

Figure 6. TEM images of (a) CoRh, (b) CuRh, (c) NiRh, and (d) NiRu nanocrystals.

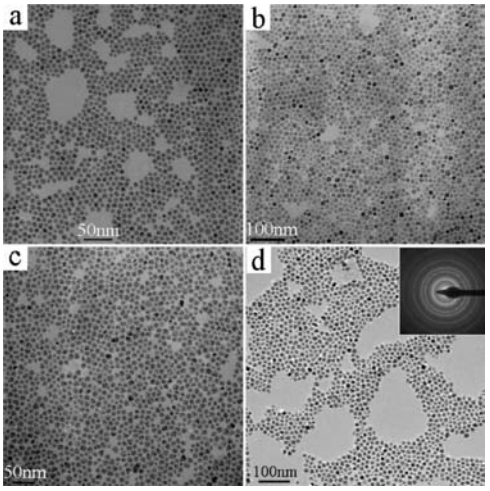

Figure 7. TEM images of (a) AgAu, (b) AgPt, (c) AuPt, and (d) AuPdPt nanocrystals.

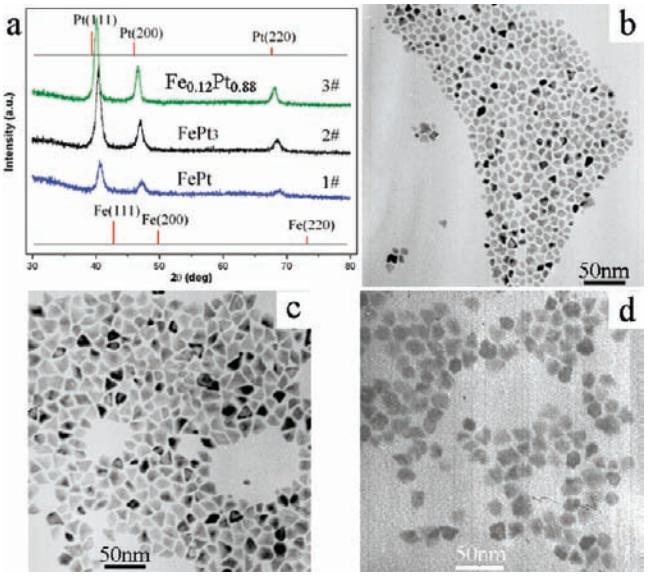

Figure 8. (a) XRD patterns of as-synthesized Fe—Pt nanomaterials and TEM images of Fe—Pt nanocrystals: (b) 1#, (c) 2#, (d) 3#.

react in the ODA system. However, when other noble metal ions and non-noble metal ions react in ODA solvent, the products are not noble metal/metal oxide nanocrystals; instead, intermetallics and alloys form (eq 5). For example, after 2:1 molar ratio of $PdCl_2$ and $Co(NO_3)_2$ were dissolved in a warm solvent of ODA, 10 min of magnetic stirring at 280 °C led to the formation of $CoPd_2$ nanocrystals. Figure S4 (Supporting Information) shows the XRD pattern of as-synthesized intermetallic $CoPd_2$ nanocrystals. The characteristic peaks match exactly with the standard JCPDS card 50-1437 of $CoPd_2$. The typical SEM image of intermetallic $CoPd_2$ nanocrystals is depicted in Figure 5a. We can see that nearly monodisperse $CoPd_2$ spheres with an average diameter of 100 nm could be obtained via this facile strategy. EDS experiment was performed on this sample. From the spectrum shown in Figure S5 (Supporting Information), we can see that only Co and Pd peaks are observed together with the Cu peak which was generated by the copper grid. From the HAADF-STEM

dx.doi.org/10.1021/ic200485v |*Inorg. Chem.* 2011, 50, 5196–5202

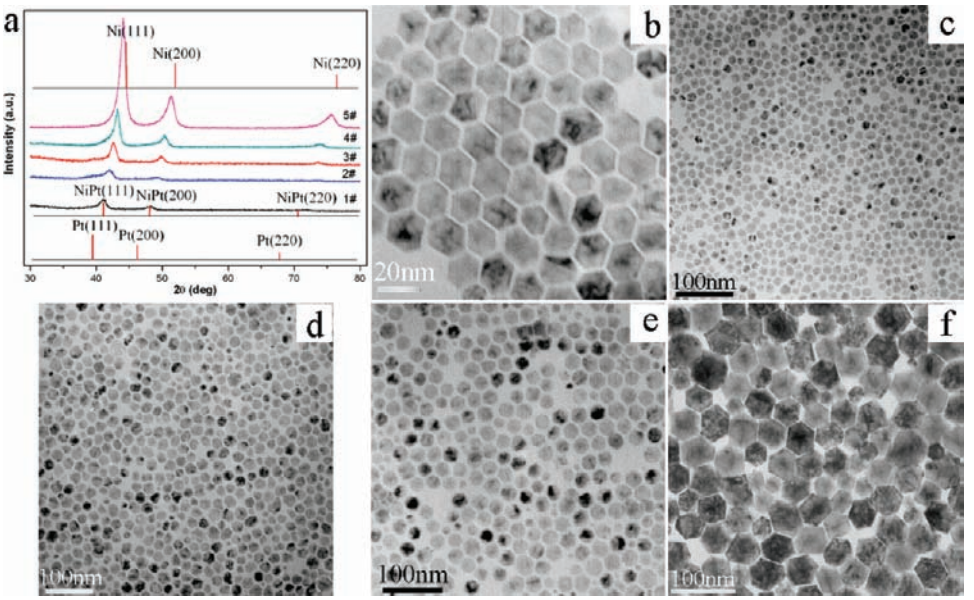

Figure 9. (a) XRD patterns of as-synthesized Ni−Pt nanomaterials and TEM images of Ni−Pt nanocrystals: (b) 1#; (c) 2#; (d) 3#; (e) 4#; (f) 5#.

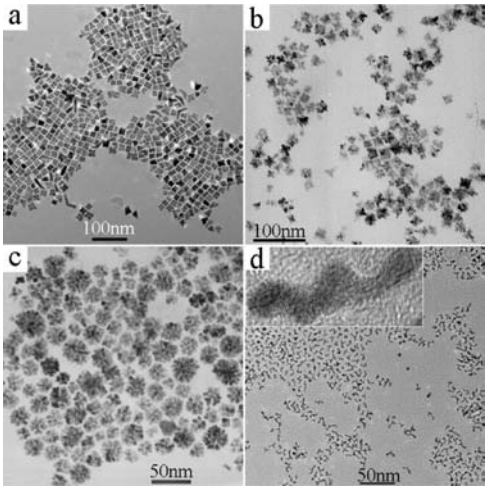

Figure 10. TEM images of $ZnPt_3$ nanocrystals with controllable morphology.

image (Figure 5b), it is clear that $CoPd_2$ spheres are composed of smaller nanoparticles. The line elemental EDS data (Figure 5c) across one single sphere show a rather homogeneous distribution of both Co and Pd in each sphere. The line-scanning profile across one single particle (Figure 5e) further confirms the homogeneous distribution of Co and Pd.

The formation of $CoPd_2$ in ODA solvent is a novel and ingenious chemical process. Why can Co^{2+} and Pd^{2+} be coreduced since Co^{2+} cannot attract electrons from ODA solvent? According to the very recent work in our group,[39c] Au^{3+} and transition metal ions (Co^{2+}, Ni^{2+}) can be coreduced in ODA solvent; that is, Au first reduced by ODA can transfer electrons from ODA to Co^{2+} or Ni^{2+} and induce their reduction. Similarly, Pd first reduced by ODA can also induce the reduction of Co^{2+} in the ODA system. After Pd and Co are reduced, the kinetic parameters lead to the formation of intermetallic $CoPd_2$. Then, various intermetallic and alloyed nanocrystals can be easily synthesized with a similar chemical process. Figure 6 shows the TEM image of as-prepared CoRh, CuRh, NiRh, and NiRu nanocrystals.

Since noble and non-noble metal ions can be coreduced by ODA solvent, it should be much easier to synthesize intermetallics and alloys of two noble metals in the ODA system. The experimental results confirmed this viewpoint. Figure S6 (Supporting Information) shows the XRD pattern of as-synthesized AgAu nanocrystals. The characteristic peaks match exactly with the standard JCPDS card 65-8424 of intermetallic AgAu. The typical TEM image of intermetallic AgAu nanocrystals is depicted in Figure 7a. We can see that nearly monodisperse AgAu nanoparticles with an average diameter of 10 nm could be obtained via this facile strategy. Similarly, AgPt, AuPt, and even trimetallic AuPdPt alloys can also be easily synthesized in this system. XRD measurements (Supporting Information, Figure S7−9) confirm the formation of these alloys, and TEM images (Figure 7b−d) show that as-obtained alloys are nearly monodisperse nanoparticles.

On the other hand, the composition, size, and morphology of intermetallic and alloyed nanocrystals could be well controlled by adjusting the reaction parameters in the ODA system. With Fe−Pt as an example, the composition was mainly controlled by the molar ratio of Fe and Pt precursors. When the molar ratio was 1:1, intermetallic FePt could be synthesized. XRD measurements were used to identify the internal crystalline structures of the products. It can be seen form Figure 8a (1#) that cubic FePt (JCPDS 65-9122) was obtained. When the molar ratio was 1:3, intermetallic $FePt_3$ could be synthesized. XRD measurement (Figure 8a, 2#) confirmed that cubic $FePt_3$ (JCPDS 29-0716) was obtained. When the molar ratio was 1:7, Fe−Pt alloy could be obtained (Figure 8a, 3#). EDS experiment was performed on Fe−Pt alloy. From the spectrum shown in Figure S10 (Supporting Information), we can see that only Fe and Pt peaks are observed together with the Cu peak which was generated by the copper grid. The composition of Fe−Pt alloy confirmed by EDS is nearly $Fe_{0.12}Pt_{0.88}$ (Supporting Information, Table S1). The size and morphology of Fe−Pt nanomaterials with different compositions were examined by TEM images. As seen in

dx.doi.org/10.1021/ic200485v |*Inorg. Chem.* 2011, 50, 5196–5202

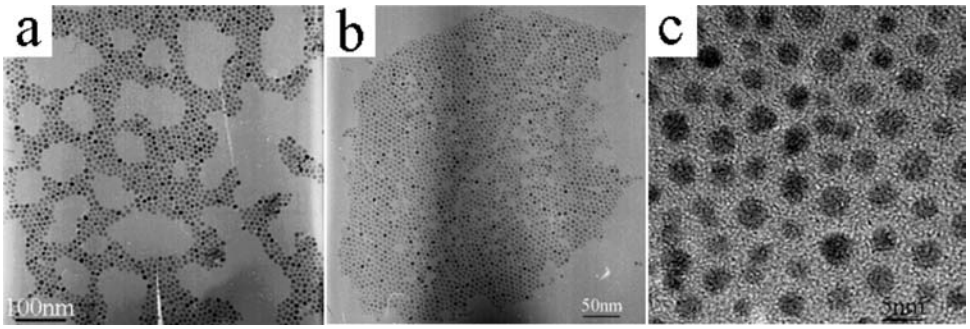

Figure 11. TEM images of $CdPt_3$ nanocrystals with controllable size.

Figure 8b−d, all the three samples display polygonal shape and their sizes increase as Pt content increases.

The experimental results for Ni−Pt nanomaterials are similar to those for Fe−Pt nanomaterials. XRD measurements were used to identify the internal crystalline structures of various Ni−Pt nanomaterials obtained with different molar ratios of Pt and Ni precursors. It can be seen from Figure 9a that, as more Ni is added, all the peaks are shifted slightly to larger 2θ values, indicative of decreased *d*-spacing and contraction of the lattice constant, due to the incorporation of increasing amounts of the smaller Ni atoms into the Pt fcc lattice. No Pt or Ni peaks appear, indicating that Ni−Pt intermetallic nanostructures or alloys formed. Figure 9b−f shows the TEM images of series of Ni−Pt nanomaterials with different compositions. All the samples display nearly monodisperse size and platelike shape. Other alloys with series of compositions could also be prepared via similar procedures. For example, we could prepare Co−Pt nanomaterials with controlled compositions by using different molar ratios of Co and Pt precursors (Supporting Information, Figure S11).

The morphology of nanocrystals was mainly controlled by experimental conditions including reaction temperature and reaction time. We employ $ZnPt_3$ as an example to show shape-controlled synthesis of intermetallic and alloyed nanocrystals. Figure S12 (Supporting Information) shows the XRD patterns of as-synthesized $ZnPt_3$ products under different conditions. For all the patterns, the peaks at 40.1°, 46.6°, and 68.1° 2θ correspond to the (111), (200), and (220) reflections of $ZnPt_3$, respectively (JCPDS 65-3257), indicating the successful synthesis of $ZnPt_3$ intermetallic compound. However, TEM results (Figure 10) show that the morphology of intermetallic $ZnPt_3$ nanocrystals obtained under different conditions are different from each other. When 1:3 molar ratio of $Zn(NO_3)_2$ and H_2PtCl_6 reacted at 240 °C for 10 min, $ZnPt_3$ nanocubes were obtained (Figure 10a). We can see that they are likely to evolve to flowers. When the reaction was performed first at 240 °C for 5 min and then at 260 °C for another 5 min, $ZnPt_3$ nanocubes could completely evolve to nanoflowers (Figure 10b). Figure 10c shows TEM image of $ZnPt_3$ nanospheres when the starting materials reacted at 260 °C for 10 min. It can be seen that these spheres consist of smaller particles. When the reaction was performed at higher temperature (280 °C) for 10 min, intermetallic $ZnPt_3$ nanocrystals with worm-like morphology could be synthesized (Figure 10d).

The size of intermetallic and alloyed nanocrystals could be controlled by the concentration of reactants. For example, after 0.01 mmol of $Cd(Ac)_2$ and 0.03 mmol of H_2PtCl_6 were dissolved in a warm solvent of ODA, 10 min of magnetic stirring at 260 °C led to the formation of $CdPt_3$ nanocrystals. Figure S13 (Supporting Information) shows the XRD pattern of as-synthesized intermetallic $CdPt_3$ (JCPDS 65-8871) nanocrystals. The typical TEM image of intermetallic $CdPt_3$ nanocrystals is depicted in Figure 11a. We can see that nearly monodisperse $CdPt_3$ nanoparticles with an average diameter of 10 nm could be obtained via this facile strategy. Increasing the concentration of reactants would lead to the formation of $CdPt_3$ nanocrystals with smaller size. When 0.02 mmol of $Cd(Ac)_2$ and 0.06 mmol of H_2PtCl_6 reacted at 260 °C for 10 min, $CdPt_3$ nanoparticles with an average diameter of 5 nm (Figure 11b) were prepared. Furthermore, $CdPt_3$ nanoparticles with an average diameter of 3 nm (Figure 11c) could be synthesized when 0.03 mmol of $Cd(Ac)_2$ and 0.09 mmol of H_2PtCl_6 reacted at 260 °C for 10 min.

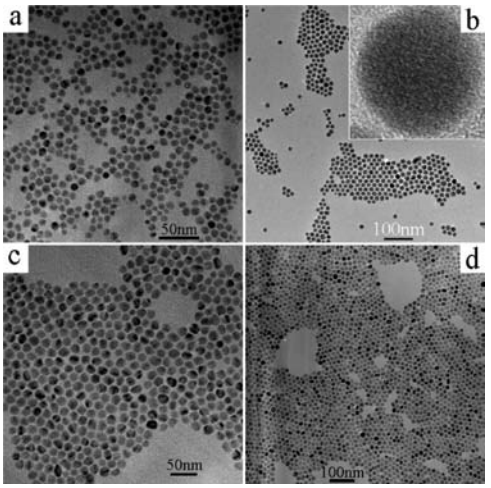

Figure 12. TEM images of CuPd nanocrystals with controllable size.

The reaction temperature and time are also key parameters in determining the size of intermetallic and alloyed nanocrystals. CuPd was employed as an example to show size-controlled synthesis of intermetallic and alloyed nanocrystals via adjusting the reaction temperature and time. After 1:1 mol ratio of $PdCl_2$ and $Cu(NO_3)_2$ were dissolved in a warm solvent of ODA, 10 min of magnetic stirring at 240 °C led to the formation of CuPd nanocrystals. XRD measurement (Supporting Information, Figure S14) confirmed the successful synthesis of CuPd intermetallic compound (JCPDS 48-1551). The typical TEM image depicted in Figure 12a shows that nearly monodisperse CuPd nanoparticles with an average diameter of 10 nm were prepared. If the reaction time was prolonged to 15 min, we could obtain intermetallic CuPd nanoparticles with larger size (∼14 nm, Figure 12b).

dx.doi.org/10.1021/ic200485v |*Inorg. Chem.* 2011, 50, 5196–5202

When the starting materials reacted at 220 °C for 10 min, CuPd nanoparticles with an average diameter of 16 nm (Figure 12c) could be synthesized. Figure 12d shows the TEM image of CuPd nanoparticles with an average diameter of 20 nm obtained when the reaction was performed at 220 °C for 15 min.

SUMMARY

In conclusion, an effective ODA synthetic system for the preparation of various nanocrystals including metals, mixed metal oxides, metal/metal oxide heterostructured nanocrystals, intermetallics, and alloys has been successfully developed in the present study. Nontoxic and inexpensive metal inorganic salts were employed as reagents. The composition, size, and morphology of nanocrystals can be easily controlled by adjusting the experimental parameters including the molar ratio of two precursors, the concentration of reactants, the reaction temperature, and time. This facile and general strategy offers the possibility of low-cost and large-scale production of various nanocrystals which can find potential applications in important fields such as environmental and industrial catalysis.

ASSOCIATED CONTENT

Supporting Information. Detailed analytical data, XRD patterns, and TEM images. This material is available free of charge via the Internet at http://pubs.acs.org.

AUTHOR INFORMATION

Corresponding Author
*E-mail: ydli@tsinghua.edu.cn.

ACKNOWLEDGMENT

This work was supported by the State Key Project of Fundamental Research for Nanoscience and Nanotechnology (2011CB932401, 2011CBA00500), NSFC (20921001, 21051001), and China Postdoctoral Science Foundation (20100470335).

REFERENCES

(1) Valden, M.; Lai, X.; Goodman, D. W. *Science* **1998**, *281*, 1647.
(2) Alivisatos, A. P. *Science* **1996**, *271*, 933.
(3) Murray, C. B.; Kagan, C. R.; Bawendi, M. G. *Annu. Rev. Mater. Sci.* **2000**, *30*, 545.
(4) El-Sayed, M. A. *Acc. Chem. Res.* **2004**, *37*, 326–333.
(5) Cui, Y.; Wei, Q. Q.; Park, H. K.; Lieber, C. M. *Science* **2001**, *293*, 1289.
(6) Tenne, R.; Margulis, L.; Genut, M.; Hodes, G. *Nature* **1992**, *360*, 444.
(7) Xie, Y.; Qian, Y. T.; Wang, W. Z.; Zhang, S. Y.; Zhang, Y. H. *Science* **1996**, *272*, 1926.
(8) Kresge, C. T.; Leonowicz, M. E.; Roth, W. J.; Vartuli, J. C.; Beck, J. S. *Nature* **1992**, *359*, 710.
(9) Li, H.; Eddaoudi, M.; O'Keeffe, M.; Yaghi, O. M. *Nature* **1999**, *402*, 276.
(10) Yang, P.; Deng, T.; Zhao, D.; Feng, P.; Pine, D.; Chmelka, B. F.; Whitesides, G. M.; Stucky, G. D. *Science* **1998**, *282*, 2244.
(11) Sun, S. H.; Murray, C. B.; Weller, D.; Folks, L.; Moser, A. *Science* **2000**, *287*, 1989.
(12) Xia, Y.; Yang, P.; Sun, Y.; Wu, Y.; Mayers, B.; Gates, B.; Yin, Y.; Kim, F.; Yan, H. *Adv. Mater.* **2003**, *15*, 353.
(13) Pan, Z. W.; Dai, Z. R.; Wang, Z. L. *Science* **2001**, *291*, 1947.
(14) Duan, X. F.; Huang, Y.; Cui, Y.; Wang, J. F.; Lieber, C. M. *Nature* **2001**, *409*, 66.
(15) Peng, X. G.; Manna, L.; Yang, W. D.; Wickham, J.; Scher, E.; Kadavanich, A.; Alivisatos, A. P. *Nature* **2000**, *404*, 59.
(16) (a) Li, X. L.; Wang, X. R.; Zhang, L.; Lee, S. W.; Dai, H. J. *Science* **2008**, *319*, 1229. (b) Jiao, L. Y.; Zhang, L.; Ding, L.; Liu, J. E.; Dai, H. J. *Nano Res.* **2010**, *3*, 387.
(17) Yin, Y. D.; Rioux, R. M.; Erdonmez, C. K.; Hughes, S.; Somorjai, G. A.; Alivisatos, A. P. *Science* **2004**, *304*, 711.
(18) (a) Xiong, Y. J.; Chen, J. Y.; Wiley, B.; Xia, Y. N. *J. Am. Chem. Soc.* **2005**, *127*, 7332. (b) Lu, X. M.; Yavuz, M. S.; Tuan, H. Y.; Korgel, B. A.; Xia, Y. N. *J. Am. Chem. Soc.* **2008**, *130*, 8900. (c) Zeng, J.; Zheng, Y. Q.; Rycenga, M.; Tao, J.; Li, Z. Y.; Zhang, Q. A.; Zhu, Y. M.; Xia, Y. N. *J. Am. Chem. Soc.* **2010**, *132*, 8552. (d) Lim, B.; Kobayashi, H.; Camargo, P. H. C.; Allard, L. F.; Liu, J. Y.; Xia, Y. N. *Nano Res.* **2010**, *3*, 180.
(19) (a) Huo, Z. Y.; Tsung, C. K.; Huang, W. Y.; Zhang, X. F.; Yang, P. D. *Nano Lett.* **2008**, *8*, 2041. (b) Habas, S. E.; Lee, H.; Radmilovic, V.; Somorjai, G. A.; Yang, P. D. *Nat. Mater.* **2007**, *6*, 692. (c) Liang, W. J.; Rabin, O.; Hochbaum, A. I.; Fardy, M.; Zhang, M. J.; Yang, P. D. *Nano Res.* **2009**, *2*, 394.
(20) Kuo, C. H.; Huang, M. H. *J. Am. Chem. Soc.* **2008**, *130*, 12815.
(21) (a) Yin, M.; O'Brien, S. *J. Am. Chem. Soc.* **2003**, *125*, 10180. (b) Yin, M.; Wu, C. K.; Lou, Y. B.; Burda, C.; Koberstein, J. T.; Zhu, Y. M.; O'Brien, S. *J. Am. Chem. Soc.* **2005**, *127*, 9506.
(22) (a) Chaubey, G. S.; Barcena, C.; Poudyal, N.; Rong, C. B.; Gao, J. M.; Sun, S. H.; Liu, J. P. *J. Am. Chem. Soc.* **2007**, *129*, 7214. (b) Wang, C.; Peng, S.; Lacroix, L. M.; Sun, S. H. *Nano Res.* **2009**, *2*, 380. (c) Mazumder, V.; Chi, M. F.; More, K. L.; Sun, S. H. *J. Am. Chem. Soc.* **2010**, *132*, 7848.
(23) Hu, M. J.; Lin, B.; Yu, S. H. *Nano Res.* **2008**, *1*, 303.
(24) Wang, L. L.; Johnson, D. D. *J. Am. Chem. Soc.* **2009**, *131*, 14023.
(25) (a) Huang, X. Q.; Zheng, N. F. *J. Am. Chem. Soc.* **2009**, *131*, 4602. (b) Wu, B. H.; Zhang, H.; Chen, C.; Lin, S. C.; Zheng, N. F. *Nano Res.* **2009**, *2*, 12. (c) Huang, X. Q.; Tang, S. H.; Zhang, H. H.; Zhou, Z. Y.; Zheng, N. F. *J. Am. Chem. Soc.* **2009**, *131*, 13916.
(26) Gu, X. H.; Xu, L. Q.; Tian, F.; Ding, Y. *Nano Res.* **2009**, *2*, 386.
(27) (a) Maksimuk, S.; Yang, S.; Peng, Z.; Yang, H. *J. Am. Chem. Soc.* **2007**, *129*, 8684. (b) Peng, Z. M.; Yang, H. *Nano Res.* **2009**, *2*, 406. (c) Wu, J. B.; Zhang, J. L.; Peng, Z. M.; Yang, S. C.; Wagner, F. T.; Yang, H. *J. Am. Chem. Soc.* **2010**, *132*, 4984.
(28) Lee, Y. W.; Kim, M.; Kim, Z. H.; Han, S. W. *J. Am. Chem. Soc.* **2009**, *131*, 17036.
(29) (a) Wang, X.; Zhuang, J.; Peng, Q.; Li, Y. D. *Nature* **2005**, *437*, 121. (b) Wang, D. S.; Xie, T.; Li, Y. D. *Nano Res.* **2009**, *2*, 30.
(30) Murray, C. B.; Norris, D. J.; Bawendi, M. G. *J. Am. Chem. Soc.* **1993**, *115*, 8706.
(31) Rockenberger, J.; Scher, E. C.; Alivisatos, A. P. *J. Am. Chem. Soc.* **1999**, *121*, 11595.
(32) Peng, Z. A.; Peng, X. G. *J. Am. Chem. Soc.* **2002**, *124*, 3343.
(33) Sun, S. H.; Zeng, H. *J. Am. Chem. Soc.* **2002**, *124*, 8204.
(34) Hyeon, T.; Lee, S. S.; Park, J.; Chang, Y.; Na, H. B. *J. Am. Chem. Soc.* **2001**, *123*, 12798.
(35) Donegá, C. M.; Liljeroth, P.; Vanmaekelbergh, D. *Small* **2005**, *1*, 1152.
(36) Zhang, Y. W.; Sun, X.; Si, R.; You, L. P.; Yan, C. H. *J. Am. Chem. Soc.* **2005**, *127*, 3260.
(37) Niederberger, M.; Garnweitner, G. *Chem.—Eur. J.* **2006**, *12*, 7282.
(38) Zhao, F.; Yuan, M.; Zhang, W.; Gao, S. *J. Am. Chem. Soc.* **2006**, *128*, 11758.
(39) (a) Wang, D. S.; Xie, T.; Peng, Q.; Li, Y. D. *J. Am. Chem. Soc.* **2008**, *130*, 4016. (b) Wang, D. S.; Xie, T.; Peng, Q.; Zhang, S. Y.; Chen, J.; Li, Y. D. *Chem.—Eur. J.* **2008**, *14*, 2507. (c) Wang, D. S.; Li, Y. D. *J. Am. Chem. Soc.* **2010**, *132*, 6280. (d) Wang, D. S.; Peng, Q.; Li, Y. D. *Nano Res.* **2010**, *3*, 574.
(40) Zheng, H. M.; Smith, R. K.; Jun, Y. W.; Kisielowski, C.; Dahmen, U.; Alivisatos, A. P. *Science* **2009**, *324*, 1309.
(41) Pauling, L. *J. Am. Chem. Soc.* **1932**, *54*, 3570.